AFTERGLOWS, REDSHIFTS, AND PROPERTIES OF *SWIFT* GAMMA-RAY BURSTS

E. Berger,[1,2,3] S. R. Kulkarni,[4] D. B. Fox,[4] A. M. Soderberg,[4] F. A. Harrison,[5] E. Nakar,[6] D. D. Kelson,[1]
M. D. Gladders,[1] J. S. Mulchaey,[1] A. Oemler,[1] A. Dressler,[1] S. B. Cenko,[4] P. A. Price,[7] B. P. Schmidt,[8]
D. A. Frail,[9] N. Morrell,[10] S. Gonzalez,[10] W. Krzeminski,[10] R. Sari,[6] A. Gal-Yam,[3,4] D.-S. Moon,[5]
B. E. Penprase,[11] R. Jayawardhana,[12] A. Scholz,[12] J. Rich,[8] B. A. Peterson,[8] G. Anderson,[8]
R. McNaught,[8] T. Minezaki,[13] Y. Yoshii,[13] L. L. Cowie,[7] AND K. Pimbblet[14]

ABSTRACT

We present optical, near-IR, and radio follow-up of 16 *Swift* bursts, including our discovery of nine afterglows and a redshift determination for three. These observations, supplemented by data from the literature, provide an afterglow recovery rate of 52% in the optical/near-IR, much higher than in previous missions (*BeppoSAX*, *HETE-2*, *INTEGRAL*, and IPN). The optical/near-IR afterglows of *Swift* events are on average 1.8 mag fainter at $t = 12$ hr than those of previous missions. The X-ray afterglows are similarly fainter than those of pre-*Swift* bursts. In the radio the limiting factor is the VLA threshold, and the detection rate for *Swift* bursts is similar to that for past missions. The redshift distribution of pre-*Swift* bursts peaked at $z \sim 1$, whereas the six *Swift* bursts with measured redshifts are distributed evenly between 0.7 and 3.2. From these results we conclude that (1) the pre-*Swift* distributions were biased in favor of bright events and low-redshift events, (2) the higher sensitivity and accurate positions of *Swift* result in a better representation of the true burst redshift and brightness distributions (which are higher and dimmer, respectively), and (3) ~10% of the bursts are optically dark, as a result of a high redshift and/or dust extinction. We remark that the apparent lack of low-redshift, low-luminosity *Swift* bursts and the lower event rate than prelaunch estimates (90 vs. 150 per year) are the result of a threshold that is similar to that of BATSE. In view of these inferences, afterglow observers may find it advisable to make significant changes in follow-up strategies of *Swift* events. The faintness of the afterglows means that large telescopes should be employed as soon as the burst is localized. Sensitive observations in *RIz* and near-IR bands will be needed to discriminate between a typical $z \sim 2$ burst with modest extinction and a high-redshift event. Radio observations will be profitable for a small fraction (~10%) of events. Finally, we suggest that a search for bright host galaxies in untriggered BAT localizations may increase the chance of finding nearby low-luminosity GRBs.

Subject heading: gamma rays: bursts

1. INTRODUCTION

The *Swift* satellite (Gehrels et al. 2004) has been operational for over 4 months, as of 2005 April. So far, about two dozen bursts have been rapidly localized to better than $10''$ accuracy thanks to the on-board X-ray telescope (XRT). Such precise and rapid positions are critical for deep ground-based follow-up, in particular for the determination of redshifts and whether a burst is optically "dark" (due to extinction within the host galaxy or attenuation by Lyman scattering from intergalactic hydrogen).

For past missions (*BeppoSAX*, *High Energy Transient Explorer 2* [*HETE-2*] WXM, *International Gamma-Ray Astrophysics Laboratory* [*INTEGRAL*], IPN), while ~90% of the afterglows were detected in the X-rays (Piro 2001; Berger et al. 2003; De Pasquale et al. 2003), the fraction with optical and radio afterglow (essential for arcsecond localization) was only 30% (e.g., Fynbo et al. 2001; Lazzati et al. 2002; Berger et al. 2002; Frail et al. 2003). Bursts localized by the Soft X-Ray Camera (SXC; Vanderspek et al. 1999) on board *HETE-2*, on the other hand, had a recovery rate in the optical of about 85% and in the radio of about 55% (Lamb et al. 2004; Berger et al. 2005c, hereafter B05). This has been attributed to the relatively accurate and rapid positions provided by the SXC and has placed the tightest limit on the fraction of dark bursts.

The current *Swift* sample of well-localized bursts is now of sufficient size to provide a meaningful comparison to past missions and to start to draw statistical inferences about the GRB population. Of particular interest is whether the increased sensitivity of *Swift* results in a sizable fraction of low-redshift,

[1] Observatories of the Carnegie Institution of Washington, 813 Santa Barbara Street, Pasadena, CA 91101.

[2] Princeton University Observatory, Peyton Hall, Ivy Lane, Princeton, NJ 08544.

[3] Hubble Fellow.

[4] Division of Physics, Mathematics, and Astronomy, 105-24, California Institute of Technology, Pasadena, CA 91125.

[5] Space Radiation Laboratory, MS 220-47, California Institute of Technology, Pasadena, CA 91125.

[6] Theoretical Astrophysics and Relativity Group, MC 130-33, California Institute of Technology, Pasadena, CA 91125.

[7] Institute for Astronomy, University of Hawaii, 2680 Woodlawn Drive, Honolulu, HI 96822.

[8] Research School of Astronomy and Astrophysics, Australian National University, Mount Stromlo Observatory, via Cotter Road, Weston Creek, ACT 2611, Australia.

[9] National Radio Astronomy Observatory, P.O. Box O, Socorro, NM 87801.

[10] Las Campanas Observatory, Carnegie Observatories, Casilla 601, La Serena, Chile.

[11] Department of Physics and Astronomy, Pomona College, 610 North College Avenue, Claremont, CA 91711.

[12] Department of Astronomy and Astrophysics, University of Toronto, 60 St. George Street, Toronto, ON M5S 3H8, Canada.

[13] Institute of Astronomy, School of Science, University of Tokyo, 2-21-1 Osawa, Mitaka, Tokyo 181-0015, Japan.

[14] Department of Physics, University of Queensland, Brisbane, 4072 Queensland, Australia.

TABLE 1
GAMMA-RAY BURST AND AFTERGLOW PROPERTIES

GRB (1)	z (2)	δt_{opt} (hr) (3)	Telescope (4)	Filter (5)	Magnitude (6)	δt_{rad} (day) (7)	$F_{\nu,rad}$ (μJy) (8)	δt_X (s) (9)	Satellite (10)	F_X (ergs cm^{-2} s^{-1}) (11)	F_γ (ergs cm^{-2}) (12)	P_γ (counts cm^{-2} s^{-1}) (13)	References GCN Circ. No. (14)
041223.................	...	14.4	LCO40	r	20.81 ± 0.15	...	...	1.63×10^4	XRT	6.5×10^{-12}	5.0×10^{-5}	7.5	B05, 2898
050117a................	...	14.6	P200/WIRC	K	>18.8	1.54	<99	193	XRT	1.8×10^{-8}	1.7×10^{-5}	0.9	B05, 2962
050124.................	...	24.5	Keck/NIRC	K	19.66 ± 0.06	4.93	<150	2.54×10^4	XRT	2.2×10^{-12}	2.1×10^{-6}	6.8	B05, 2973
050126.................	1.290	4.32	Keck/NIRC	K	19.45 ± 0.17	2.09	<90	200	XRT	2.5×10^{-11}	2.0×10^{-6}	0.4	B05, 2987
050128.................	...	11.4	Faulkes	R	>20.5	11.3	<93	873	XRT	2.6×10^{-12}	4.5×10^{-6}	4.6	2991, 2992, 3001, 3011
050215b................	...	9.00	P60	R	>20.5	3.39	<93	5.7×10^3	XRT	few $\times 10^{-13}$	4.5×10^{-7}	...	3032, 3034, 3035, 3053, 3066
		9.76	UKIRT/UFTI	K	20.23 ± 0.11								3028, 3031
050219a................	...	2.05	MJUO 0.6-m	R	>20.5	...	...	...	...	...	9.4×10^{-6}	5.5	3038, 3041
	...	17.7	LCO40	I	>21.5								3048
050219b................	...	4.32	VLT/FORS2	R	>23.0	...	...	...	...	...	2.3×10^{-5}	26	3044, 3064
	...	5.21	LCO100	K	19.5 ± 0.12								This paper
050223.................	...	4.10	PROMPT	R	>21.2	...	...	7.67×10^4	*XMM*	4.5×10^{-14}	7.4×10^{-7}	0.8	3055, 3067, 3109
		5.22	LCO40	R	>21.6								This paper
050306.................	...	50.5	TNG	R	>23.0	8.27	<84	1.30×10^5	XRT	3.0×10^{-14}	1.9×10^{-5}	2.4	3089, 3092
050315.................	1.950	11.6	Mag./LDSS3	R	20.9 ± 0.10	0.81	300 ± 62	...	...	...	4.2×10^{-6}	2.5	3098, 3100, 3101, 3102, 3105
050318.................	1.444	8.15	Mag./IMACS	R	20.6 ± 0.08	...	...	7.7×10^3	XRT	7.0×10^{-12}	2.1×10^{-6}	3.8	3112, 3114, 3122, 3134
050319.................	3.240	8.70	RTT150	R	20.14 ± 0.10	0.63	<174	...	...	...	8.0×10^{-7}	1.7	3119, 3127, 3132, 3136
050326.................	...	6.90	MJO 0.6-m	I	>20.3	...	...	5.4×10^4	*XMM*	7.4×10^{-13}	1.9×10^{-5}	17	3145, 3151, 3293
050401.................	2.900	0.96	SSO40	R	20.3 ± 0.08	5.69	122 ± 33	1.9×10^4	XRT	3.8×10^{-12}	1.9×10^{-5}	14	3163, 3164, 3176, 3179, 3187
050406.................	...	7.80	Mag./LDSS3	R	22.0 ± 0.09	...	...	3.8×10^4	XRT	6.7×10^{-14}	9.0×10^{-8}	3.2	3183, 3184, 3185
050410.................	...	4.45	ARIES	R	>20.5	0.21	<171	1.9×10^3	XRT	4.0×10^{-12}	6.9×10^{-6}	2.0	3219, 3223, 3226
	...	15.6	P60	i	>21.5								3231
050412.................	...	0.22	P60	R	>20.0	3.88	<57	5.0×10^3	XRT	3.9×10^{-12}	2.1×10^{-6}	0.8	3242, 3251, 3253, 3277
		0.83	LCO100	R	>22.4								This paper
050416a................	0.653	3.50	SSO 2.3 m	R	21.7 ± 0.10	5.58	260 ± 55	4.3×10^4	XRT	2.8×10^{-13}	3.8×10^{-7}	4.8	3266, 3273, 3275, 3318
050416b................	...	1.10	Mag./IMACS	R	>24.0	...	...	...	...	...	2.1×10^{-6}	7.9	3282, 3284
050421.................	...	4.62	P60	R	>22.0	0.44	<102	837	XRT	6.4×10^{-13}	1.8×10^{-7}	0.5	3299, 3301, 3305, 3308
		1.70	TNG	K	>18.6								3300
		9.30	MAGNUM	J	>20.3								3313
050408[a]...............	1.236	3.70	RTT150	R	20.94 ± 0.10	2.53	<87	2.1×10^4	XRT	6.2×10^{-12}	3.3×10^{-6}	...	3189, 3191, 3201, 3234, 3262

NOTES.—Prompt emission and afterglow properties for all *Swift* bursts with XRT positions and ground-based follow-up as of the end of April 2005. The columns are (1) GRB name, (2) redshift, (3) time of optical /near-IR observation, (4) telescope, (5) filter, (6) optical /near-IR magnitude, (7) time of radio observation, (8) radio flux at 8.46 GHz, (9) time of X-ray observation, (10) X-ray satellite, (11) X-ray flux, (12) γ-ray fluence, (13) γ-ray peak flux, and (14) references; B05 is Berger et al. (2005c); all other references are GCN Circular numbers.
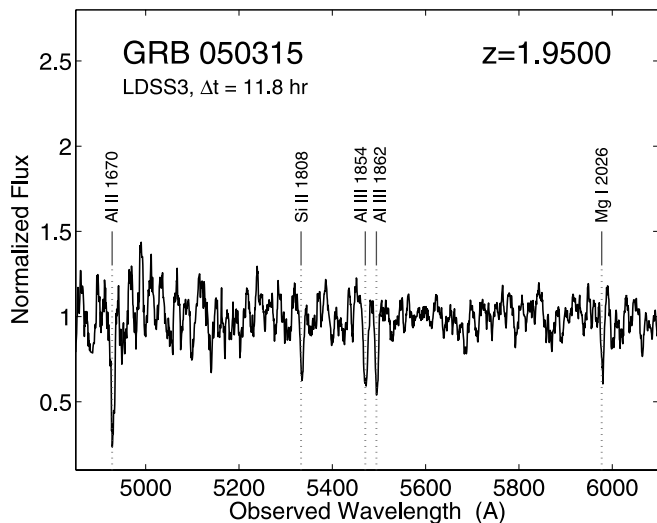
[a] *HETE-2* SXC burst.

FIG. 1.—Absorption spectrum of GRB 050315 taken with the LDSS3 instrument on the Magellan/Clay 6.5 m telescope 11.8 hr after the burst ($R = 20.9$ mag; Table 1). The spectrum exhibits several absorption features corresponding to Al II (λ1670), Si II (λ1808), Al III ($\lambda\lambda$1854, 1862), and Mg I (λ2026) at a redshift $z = 1.9500 \pm 0.0008$.
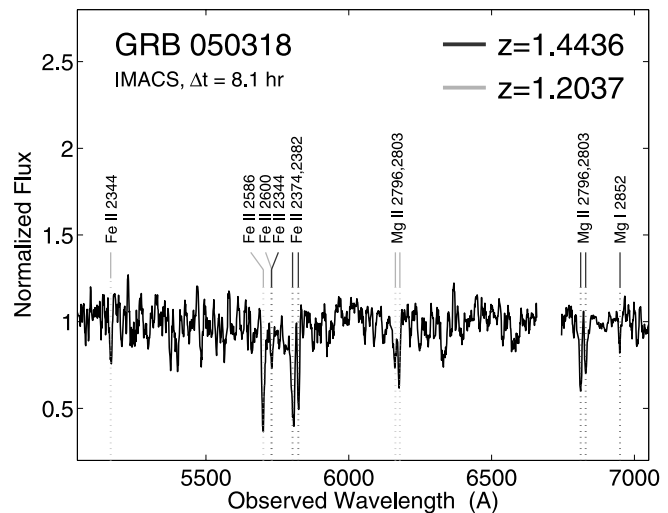

FIG. 2.—Absorption spectrum of GRB 050318 taken with the IMACS instrument on the Magellan/Baade 6.5 m telescope 8.1 hr after the burst ($R = 20.6$ mag; Table 1). The spectrum exhibits several absorption features corresponding to Fe and Mg lines at redshifts $z_1 = 1.2037 \pm 0.0004$ and $z_2 = 1.4436 \pm 0.0009$. We identify the higher redshift system with GRB 050318.

low-luminosity GRBs or an increase in the detection rate of GRBs at higher redshifts. A related question is whether the recovery rate of optical/near-IR afterglows is close to unity.

Here we present our comprehensive optical/near-IR and radio follow-up observations of *Swift* bursts. Of the 21 *Swift* GRBs with XRT positions and ground-based follow-up, we observed a total of 16 in the optical/near-IR and 13 in the radio. We discovered nine of the 12 optical/near-IR afterglows to date and radio afterglows for three bursts, and we determined the redshifts of three *Swift* bursts and one SXC burst. We show that the optical/near-IR detection rate for *Swift* bursts is indeed higher than in past missions, but that the afterglows are significantly fainter, and their redshifts tend to be higher. Deep limits suggest that ~10% of the *Swift* bursts are optically dark. These conclusions have major ramifications for future follow-up efforts, which we discuss toward the end of the paper.

2. AFTERGLOW DISCOVERY AND REDSHIFTS

Follow-up observations by our group were made using an armada of telescopes at the following facilities: Las Campanas Observatory (LCO), Magellan, Palomar Observatory, Keck, Siding Spring Observatory (SSO), and the Very Large Array (VLA).[15] Afterglow discovery and follow-up of GRBs 041223, 050117a, 050124, and 050126 were detailed in B05. In Table 1 we provide photometry and radio flux measurements for subsequent events, augmented by relevant data from the literature.

All optical/near-IR observations were reduced in the standard manner using IRAF routines. Astrometry was performed relative to the USNO-B catalog, and the afterglow identifications were made by comparison to the Digitized Sky Survey (DSS) or through detection of a fading behavior. The VLA radio observations were undertaken in the standard continuum mode, and the data were reduced and analyzed using the Astronomical Image Processing System.

We used the LDSS3 and IMACS spectrographs on the Magellan 6.5 m telescopes to obtain absorption spectra for the *Swift*

GRBs 050315 (Fig. 1) and 050318 (Fig. 2), and the *HETE-2* SXC burst GRB 050408 (Fig. 3). We also used ESI on the Keck II telescope to obtain a redshift for the host galaxy of GRB 050126 (B05). In all cases, we used standard IRAF routines to bias-subtract and flatfield the data, while rectification and sky subtraction were performed using the method and software described in Kelson (2003). Air-to-vacuum and heliocentric corrections were applied to the wavelength calibration. The redshifts determined from these spectra are listed in Table 1, along with two other redshifts available from the literature. A detailed analysis of the absorption spectra will be provided in a separate paper (E. Berger et al. 2005, in preparation).

Finally, we list in Table 1 the X-ray fluxes and γ-ray peak photon fluxes and fluences when available from the literature. For
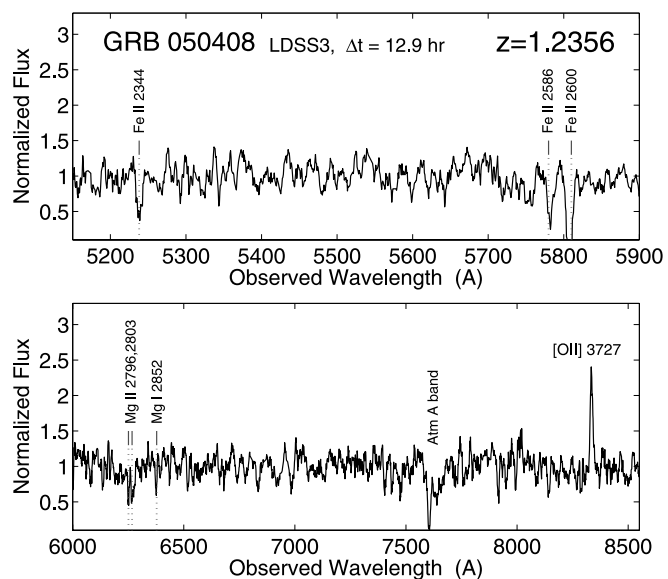

FIG. 3.—Absorption spectrum of the *HETE-2* SXC burst GRB 050408 taken with the LDSS3 instrument on the Magellan/Clay 6.5 m telescope about 12.9 hr after the burst ($R = 22.0$ mag). The spectrum exhibits absorption from Fe and Mg, as well as an [O II] λ3727 emission line. The redshift of the burst is $z = 1.2356 \pm 0.0008$.

GRBs 050401, 050406, 050416a, and 050421 we undertook our own analysis of the XRT data (from the *Swift* archive).[16] We cleaned the data using the standard settings in xrtpipeline, with the standard event grade selection, and extracted photons in the 0.5–7 keV band. This optimizes detection signal-to-noise for the average afterglow, which has a photon spectral index of about −2. For the photon counting mode we used an extraction radius of 20 pixels (90% encircled energy) for the source and an annulus outside of this, starting at a radius of 30 pixels, for background extraction. The data were fit with a power law plus absorption; none of the sources exhibit absorption in excess of the Galactic value. Finally, we used the measured photon spectral index to extrapolate the flux to the 2–10 keV band for comparison with bursts from other missions. The conversion from count rate to flux is 1 count $s^{-1} = 2 \times 10^{-11}$ ergs cm^{-2} s^{-1} (2–10 keV).

3. THE PROPERTIES OF *Swift* BURSTS

In this section we summarize the properties of the sample of 21 *Swift* bursts that have XRT positions and ground-based optical/near-IR follow-up (Table 1; as of the end of 2005 April). We compare the *Swift* sample with two previous samples: (1) *HETE-2* SXC bursts with positional accuracy better than 2′ ("SXC") and (2) bursts localized by other past missions (*BeppoSAX*, *HETE-2* WXM, IPN, and *INTEGRAL* ["BWI"]). The former sample (14 objects) enjoys superior localizations, while the latter sample (96 objects) has moderate localizations (∼3′–30′).

The overall detection fraction of X-ray afterglows for *Swift* bursts is 21/22 (one burst detected in γ-rays has no XRT detection). This is essentially the same as the detection fraction for past missions of about 90%. The recovery fraction of optical/near-IR afterglows for the *Swift* sample, 11/21 ≈ 52%, is significantly higher than the 30% recovery fraction of the BWI sample, but is worse than the 85% fraction for the SXC bursts.

In Figure 4 we plot the *R*-band magnitudes for the three samples, normalized to *t* = 12 hr. We extrapolate (or interpolate) to the fiducial time (and for near-IR afterglows to the fiducial band) using the measured temporal and spectral slopes or by conservatively assuming[17] $F_\nu \propto t^{-0.9}\nu^{-0.6}$. As can be seen from Figure 4, the *Swift* afterglows, with a mean $\langle R \rangle = 21.6$ mag, are fainter than the SXC and BWI samples by about 1.8 mag. In fact, while 40% of all afterglows from past missions had $R < 19$ mag at $t = 12$ hr, not a single *Swift* burst falls in that bright category. Formally, the Kolmogorov-Smirnov (K-S) test reveals that the probability that the *Swift* bursts are drawn from the SXC sample (not including the bright, low-redshift GRB 030329) and the BWI sample is only 1.2% and 0.2%, respectively.

We carry out a similar exercise for the X-ray afterglow emission (Fig. 5). The X-ray fluxes at $t = 12$ hr are estimated using the measured decay indices (when available) or the mean value based on all bursts, $\langle \alpha_X \rangle = -1.3$; for XRT fluxes measured in the first hour we use a more conservative $\alpha_X = -1$. As with the optical/near-IR afterglows, the X-ray afterglows of *Swift* bursts are fainter than those of the other two samples by
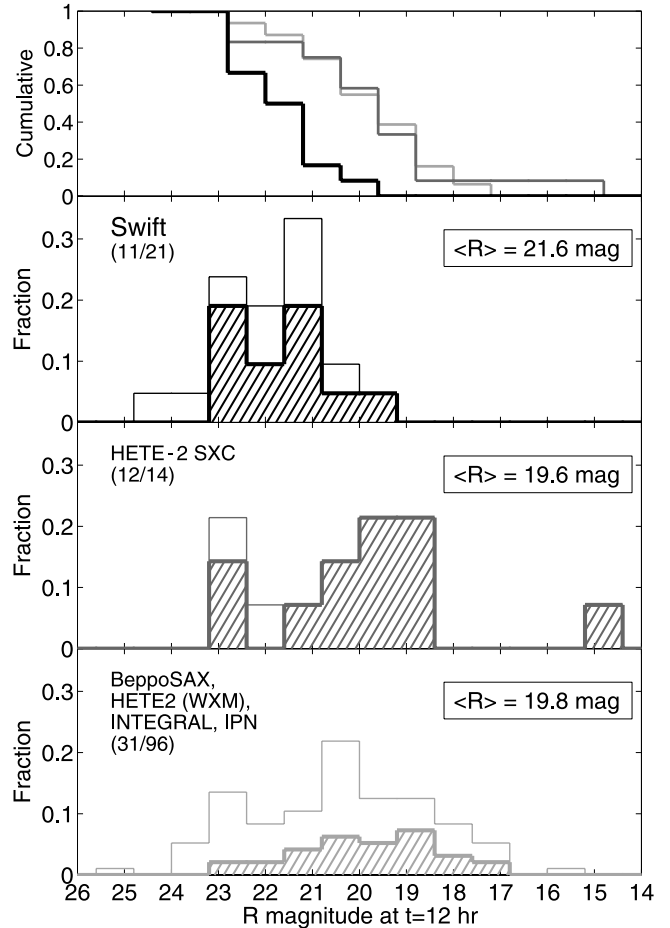

Fig. 4.—Histograms of optical *R*-band magnitudes (corrected for Galactic extinction) extrapolated to a common time of 12 hr after the burst for the *Swift*, SXC, and BWI samples. For GRBs 041223, 050124, 050126, 050215b, 050319, 050401, and 050416a we use the measured decay rates; for all other bursts we use $F_\nu \propto t^{-0.9}$. Shaded regions are detections, while thin histograms include all upper limits. The mean *R* magnitude of the detections in each sample is given as $\langle R \rangle$. The top panel shows the cumulative distributions. The afterglows of *Swift* bursts are fainter than those of bursts detected in previous missions. This is primarily the result of accurate and rapid localizations, which have allowed us to increase the recovery rate through the detection of fainter objects, and the lower threshold of *Swift* (Fig. 8), which results in detection of fainter bursts. The SXC sample, with a detection rate of ∼85% in the optical, contains many bright afterglows, suggesting a bias in favor of bright bursts.

about a factor of 5. A K-S test indicates a probability of only 5% and 0.1% that the *Swift* bursts are drawn from the SXC and BWI samples, respectively.

We additionally use the X-ray fluxes, extrapolated to the optical band, to determine which bursts are dark. Using $F_\nu \propto \nu^{-0.6}$, based on optical/X-ray detections, we find that of the six bursts with optical limits and X-ray detections, one (050412) is expected to be at least 1 mag brighter than the measured limits. This suggests that the fraction of dark bursts is at least 10%, and perhaps as high as 1/3.

Our comprehensive radio follow-up of 13 *Swift* bursts led to the detection of only three (GRBs 050315, GRB 050401, GRB 050416a; Fig. 6). This is comparable to the 30% recovery fraction of the BWI sample, but is lower than the 55% recovery of the SXC sample.

The redshift distribution of *Swift* bursts differs from that of the BWI sample, which peaks at $z \sim 0.8$ (Fig. 7). In fact, the flat distribution of *Swift* bursts is similar to that of the SXC sample. It is interesting to note that five of the six redshifts of the (admittedly

---

[16] See http://heasarc.gsfc.nasa.gov/docs/swift/archive.
[17] The choice of spectral and temporal indices is appropriate for the case of spherical geometry, a constant density circumburst environment, an electron power law index $p = 2.2$, and a synchrotron cooling frequency $\nu_c > \nu_R$. This provides the most conservative decay rate: for a wind medium the dependence is $t^{-1.4}$, for $\nu_c < \nu_R$ it is $t^{-1.15}$, and for the case of a collimated explosion it is $t^{-p} \sim t^{-2.2}$.
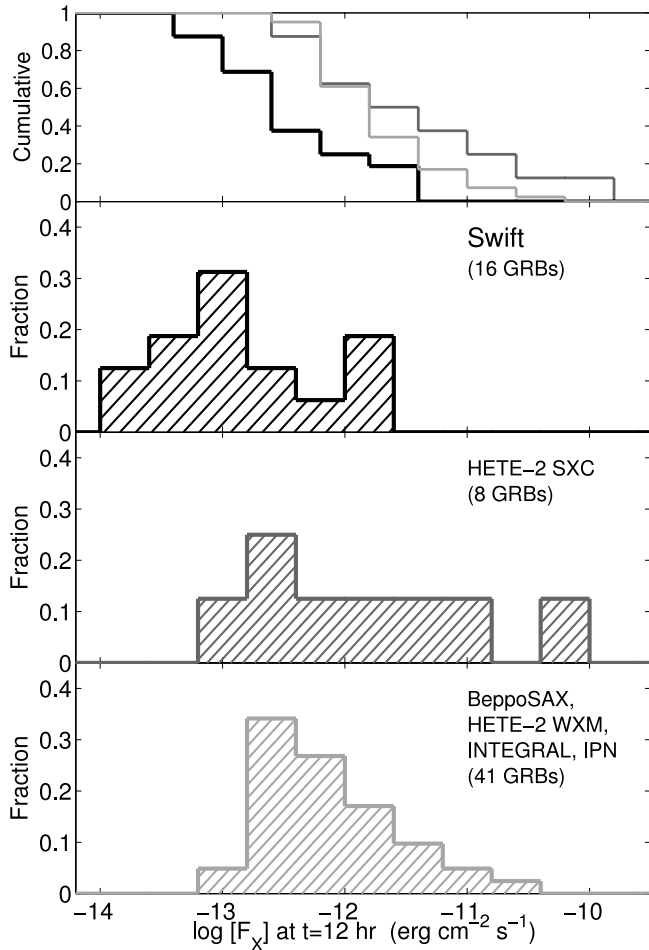
FIG. 5.—Histograms of X-ray fluxes extrapolated to a common time of 12 hr after the burst for the *Swift*, SXC, and BWI samples. For GRBs 050215b, 050401, 050406, and 050416a we use the measured decay rates; for all other bursts we use the mean value $\langle\alpha_X\rangle = -1.3$. The top panel shows a cumulative distribution. The distribution for pre-*Swift* bursts is from Berger et al. (2003) and B05. The X-ray afterglows of *Swift* bursts are fainter than those of bursts detected in previous missions. Since the past recovery rate was already about 90%, this suggests that the lower trigger threshold of *Swift* than *BeppoSAX* and *HETE-2* is giving rise to fainter and higher redshift bursts.

FIG. 6.—Detections (*circles*) and upper limits (*triangles*) in the radio for *Swift* bursts. Also shown are the radio light curve of GRB 990123, which was dominated by reverse shock emission, and synthetic light curves of the forward shock emission from a burst with typical parameters ($n_0 = 3$ cm^{-3}, $\epsilon_e = 0.1$, and $\epsilon_B = 0.01$) placed at $z = 2$ and with blast wave energies of 1×10^{52} ergs (*thick line*) and 3×10^{51} ergs (*thin line*). Clearly, if *Swift* bursts typically have fainter afterglows (e.g., less energy), as indicated by their optical and X-ray fluxes, the majority may be too faint to detect at the VLA sensitivity.

small) *Swift* sample are beyond 1.25, while the median redshift for pre-*Swift* bursts is 1.05.

To summarize, *Swift* bursts, relative to both the BWI and SXC samples, have fainter X-ray and optical afterglows. *Swift* and the BWI sample have a similar and low (30%) recovery fraction for radio afterglows. We explain these findings as follows. The BWI sample with its moderate localization precision favored brighter afterglows, which in turn favored lower redshift events. The *Swift* XRT positions, combined with a greater trigger sensitivity (Fig. 8), allow us to increase the detection fraction and hence to find fainter and higher redshift events. The low rate of radio recovery is primarily a result of the VLA sensitivity (which is lower relative to the optical/near-IR bands). The accurate and faster positions available from *Swift* do not help to increase the radio detection fraction. In fact, the fainter afterglows of *Swift* bursts may in the long run result in a lower recovery fraction in the radio (Fig. 6).

The statistics of the SXC sample, however, are puzzling. The high afterglow detection fraction for SXC bursts, and their flat redshift distribution (unlike the BWI sample), can be attributed to better localizations. However, with a higher recovery rate we
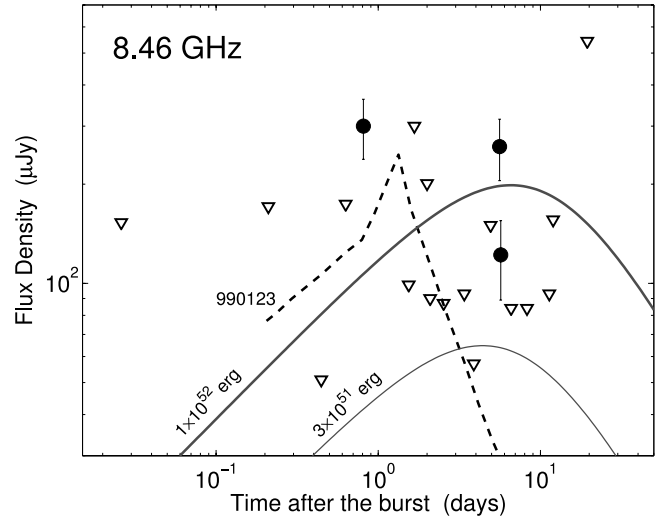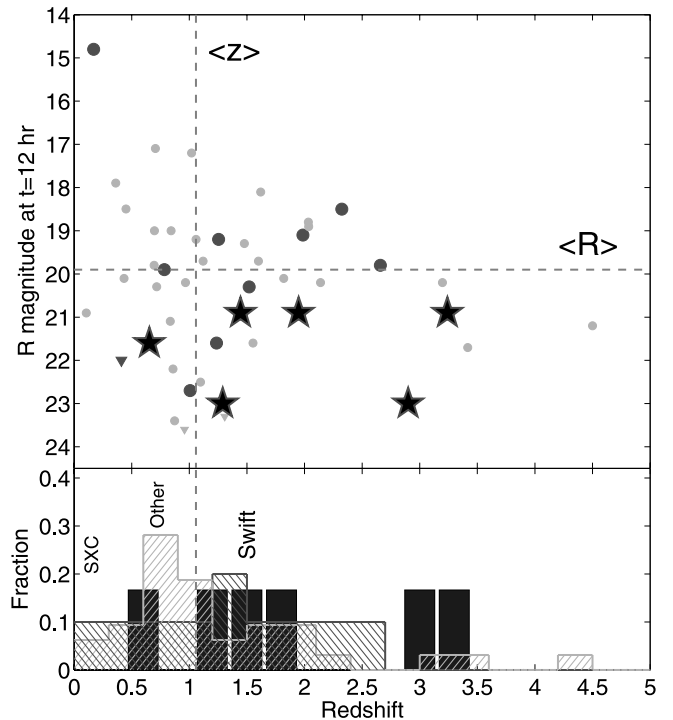

FIG. 7.—Optical *R*-band magnitudes (corrected for Galactic extinction) extrapolated to a common time of 12 hr after the burst, plotted against redshift. Light gray circles designate BWI bursts, dark gray circles represent SXC bursts, and stars are for *Swift* bursts. The dashed lines designate the median magnitude and redshift for all pre-*Swift* bursts. The higher redshifts of *Swift* bursts are the result of deeper and faster searches, which uncover fainter afterglows, as well as the lower threshold of *Swift*.
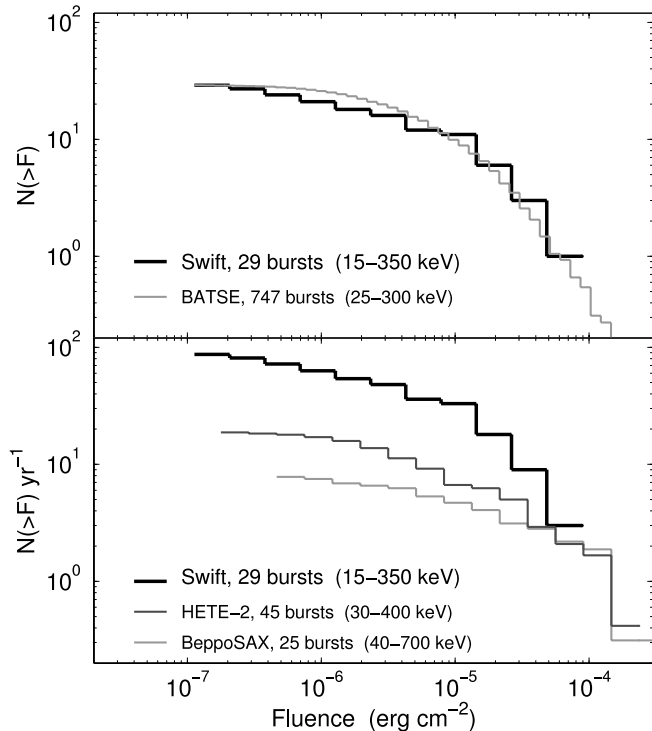
031203? Separately, many astronomers are poised to exploit the brilliance of the afterglows to investigate the star formation history of the universe, probe the intergalactic medium in the early universe, and investigate the build-up of elements in the disks of galaxies. For these astronomers the following questions are of prime importance: What is the fraction of dark bursts, and how many of these lie at high redshift ($z > 6$)? Will the afterglows be bright enough to undertake high resolution optical/near-IR spectroscopy? What is the annual *Swift* rate of such interesting bursts? We believe that our investigation of the current sample has started to address some aspects of the above questions.

To start with, the observed *Swift* rate is about 80–90 bursts per year. This is less than the 150 bursts per year estimated from prelaunch simulations, which assumed a threshold of 5 times better than that of BATSE (Fenimore et al. 2004). The smaller rate is consistent with the fact that the fluences and peak count rates of the observed *Swift* events are in fact similar to those that triggered BATSE, as are the resulting threshold and the $\log N/ \log S$ distribution (Fig. 8).

Next, there is at present no indication of a large sample of nearby ($z \lesssim 0.2$) low-luminosity events. As noted earlier, the lowest measured redshift is $z \approx 0.65$. More importantly, there is no evidence of bright galaxies[18] in the XRT error circles. The lack of low-redshift objects is not surprising given that *Swift*'s threshold is similar to that of BATSE. In the BATSE sample, even when including the faint, nontriggered bursts, the limit on a contribution from a spatially homogeneous local population is about 7% (90% confidence; Kommers et al. 2000).

In addition, the *Swift* afterglows are fainter and their redshifts are higher. The rapid response of a variety of telescopes to *Swift* events, and their accurate positions, means that the *Swift* sample has the least bias (relative to the previous samples). We therefore conclude that (1) the true GRB population peaks at a higher redshift than indicated by pre-*Swift* bursts, $z \gtrsim 2$, and (2) the typical optical and X-ray afterglows are faint: at $t = 12$ hr, $R \sim 21.5$ mag and $F_X \sim 3 \times 10^{-13}$ ergs cm^{-2} s^{-1}, respectively.

A number of ramifications follow from the above discussion. First, the fainter afterglows mean that it is critical that moderate (and large) telescopes be pressed into service to identify optical/near-IR afterglows; the expected signal level (at $t = 15$ minutes) of $R \sim 17.7$ mag, $J \sim 16.6$ mag, and $K \sim 15.2$ mag is difficult to achieve on small robotic telescopes. In addition, the combination of higher redshifts and fainter afterglows strongly favor longer wavelength observations (RIz bands vs. UBV); indeed, a simple way to improve the current low detection fraction by the UVOT (5/16) is to observe in only the V band (unless the afterglow is noted to be bright). Finally, near-IR observations are essential to distinguish dusty events from high-redshift events.

So far we have tacitly assumed that *Swift* events are representative of the true sample, and the afterglow and redshift distributions are simply due to a lower threshold and better localizations than *BeppoSAX* and *HETE-2*. However, a possible bias arises from the softer band of the BAT (15–150 keV) compared to the *BeppoSAX* GRBM (40–700 keV) and *HETE-2* FREGATE (6–400 keV) instruments. Amati et al. (2002) and Sakamoto et al. (2005) show that there is a correlation between the peak energy of the prompt emission spectrum, E_{peak}, and the fluence (or peak flux). This is an approximate relation but it appears to be obeyed in the mean. This means that the BAT is well suited for

Fig. 8.—*Top:* $\log N/ \log F$ for *Swift* bursts with published fluences compared to a sample of BATSE bursts for which a fluence measurement is available in all four channels and the error is smaller than half of the measured value. The BATSE fluence distribution is normalized by the relative number of bursts. The similarity of the distributions and thresholds explain the lack of local, low-luminosity bursts in the current *Swift* sample, as well as the lower event rate compared to prelaunch estimates (90 vs. 150 per year, respectively). *Bottom:* The same *Swift* sample but compared to *BeppoSAX* and *HETE-2* bursts (Amati et al. 2002; Sakamoto et al. 2004; Ghirlanda et al. 2005). For *HETE-2* we included only GRBs and X-ray rich GRBs. Each sample is normalized by the approximate detection rates per year. Clearly, *Swift* has a lower threshold and this results primarily in an increase in the number of faint bursts.

would expect the SXC afterglows to be fainter than those of the BWI sample, while they are in fact just as bright. Similarly, the recovery fraction of radio afterglows, which is set by the VLA threshold, is expected to be comparable to that of the BWI and *Swift* samples; it is instead significantly higher.

There are two possible explanations. Either the SXC sample is suffering severely from Poisson statistics (although this is unlikely), or the sample is biased to brighter afterglows. We speculate that soft X-ray contribution from the very early afterglow or excess soft X-ray emission in the prompt phase (e.g., Vanderspek et al. 2004) may enhance detection by the SXC and possibly give rise to a sample with brighter afterglows. It appears that the SXC sample may not serve as a proxy for the true distribution of afterglow properties, including the fraction of dark bursts.

4. DISCUSSION AND RAMIFICATIONS

Swift has been in orbit for 6 months and has localized 32 bursts as of the end of 2005 April. In this paper we presented the results of our ground-based optical/near-IR and radio follow-up programs of the 21 bursts with accurate positions from the XRT, including the determination of three redshifts.

There is high expectation among astronomers that *Swift*, over the remaining 30 months of its prime phase, will help address several major questions: Are *Swift* bursts representative of the overall GRB population? How do GRBs evolve with redshift? Is there a large population of nearby events like GRBs 980425 and

---

[18] In the host galaxy sample for pre-*Swift* GRBs, all objects at $z < 0.5$ have $R \lesssim 22$ mag and a mean of 20.6 mag. Similar hosts should have been detected in most of the afterglow searches of *Swift* XRT positions (Table 1).

finding "X-ray–rich GRBs," which will therefore result in selection of bursts with a lower fluence and peak flux. This is potentially a significant bias in the *Swift* sample. Conversely, the softer triggering band of the BAT means that the detection of short-hard bursts will be diminished. This may explain why *Swift* has localized only two short-hard bursts out of the sample of 41 bursts.

The aggregate effect of *Swift*'s trigger threshold, energy band, and localization accuracy has resulted in a sample that is dominated by faint optical/near-IR and X-ray afterglows with seemingly higher redshifts than indicated by past missions. The current recovery rate suggests that as many as 1/3 of all *Swift* bursts may be optically dark. Therefore, while a local population of low-energy bursts does not contribute significantly to the sample, the possibility that *Swift* will uncover a larger population of high-redshift bursts than past missions remains open. Follow-up efforts and resources should be focused on this possibility.

REFERENCES

Amati, L., et al. 2002, A&A, 390, 81
Anderson, G., et al. 2005, GCN Circ. 3266, http://gcn.gsfc.nasa.gov/gcn/gcn3/3266.gcn3
Antonelli, L. A., et al. 2005, GCN Circ. 2991, http://gcn.gsfc.nasa.gov/gcn/gcn3/2991.gcn3
Barthelmy, S., et al. 2005, GCN Circ. 2962, http://gcn.gsfc.nasa.gov/gcn/gcn3/2962.gcn3
Berger, E., Gladders, M., & Oemler, G. 2005, GCN Circ. 3201, http://gcn.gsfc.nasa.gov/gcn/gcn3/3201.gcn3
Berger, E., & Gonzalez, S. 2005, GCN Circ. 3048, http://gcn.gsfc.nasa.gov/gcn/gcn3/3048.gcn3
Berger, E., Kulkarni, S. R., & Frail, D. A. 2003, ApJ, 590, 379
Berger, E., & Mulchaey, J. 2005, GCN Circ. 3122, http://gcn.gsfc.nasa.gov/gcn/gcn3/3122.gcn3
Berger, E., Mulchaey, J., Morrell, N., & Krzeminski, W. 2005a, GCN Circ. 3282, http://gcn.gsfc.nasa.gov/gcn/gcn3/3282.gcn3
Berger, E., Oemler, G., & Gladders, M. 2005b, GCN Circ. 3185, http://gcn.gsfc.nasa.gov/gcn/gcn3/3185.gcn3
Berger, E., et al. 2002, ApJ, 581, 981
———. 2005c, ApJ, 629, 328 (B05)
Bikmaev, I., et al. 2005, GCN Circ. 3262, http://gcn.gsfc.nasa.gov/gcn/gcn3/3262.gcn3
Capalbi, M., et al. 2005, GCN Circ. 3184, http://gcn.gsfc.nasa.gov/gcn/gcn3/3184.gcn3
Cenko, S. B., et al. 2005a, GCN Circ. 3231, http://gcn.gsfc.nasa.gov/gcn/gcn3/3231.gcn3
———. 2005b, GCN Circ. 3266, http://gcn.gsfc.nasa.gov/gcn/gcn3/3266.gcn3
———. 2005c, GCN Circ. 3299, http://gcn.gsfc.nasa.gov/gcn/gcn3/3299.gcn3
Cummings, J., et al. 2005a, GCN Circ. 2973, http://gcn.gsfc.nasa.gov/gcn/gcn3/2973.gcn3
———. 2005b, GCN Circ. 2992, http://gcn.gsfc.nasa.gov/gcn/gcn3/2992.gcn3
———. 2005c, GCN Circ. 3044, http://gcn.gsfc.nasa.gov/gcn/gcn3/3044.gcn3
———. 2005d, GCN Circ. 3145, http://gcn.gsfc.nasa.gov/gcn/gcn3/3145.gcn3
Cusumano, G., et al. 2005, GCN Circ. 3275, http://gcn.gsfc.nasa.gov/gcn/gcn3/3275.gcn3
D'Avanzo, P., et al. 2005a, GCN Circ. 3064, http://gcn.gsfc.nasa.gov/gcn/gcn3/3064.gcn3
———. 2005b, GCN Circ. 3089, http://gcn.gsfc.nasa.gov/gcn/gcn3/3089.gcn3
De Luca, A., Gotz, D., & Campana, S. 2005a, GCN Circ. 3293, http://gcn.gsfc.nasa.gov/gcn/gcn3/3293.gcn3
De Luca, A., et al. 2005b, GCN Circ. 3109, http://gcn.gsfc.nasa.gov/gcn/gcn3/3109.gcn3
De Pasquale, M., et al. 2003, ApJ, 592, 1018
de Ugarte Postigo, A., Eguchi, S., Gorosabel, J., Yock, P., & Castro-Tirado, A. J. 2005, GCN Circ. 3041, http://gcn.gsfc.nasa.gov/gcn/gcn3/3041.gcn3
Fenimore, E. E., et al. 2004, Baltic Astron., 13, 301
———. 2005, GCN Circ. 3219, http://gcn.gsfc.nasa.gov/gcn/gcn3/3219.gcn3
Frail, D. A., Kulkarni, S. R., Berger, E., & Wieringa, M. H. 2003, AJ, 125, 2299
Frail, D. A., et al. 2005, GCN Circ. 3011, http://gcn.gsfc.nasa.gov/gcn/gcn3/3011.gcn3
Fugazza, D., et al. 2005, GCN Circ. 3300, http://gcn.gsfc.nasa.gov/gcn/gcn3/3300.gcn3
Fynbo, J. U., Hjorth, J., Jensen, B. L., Jakobsson, P., Moller, P., & Naranen, J. 2005a, GCN Circ. 3136, http://gcn.gsfc.nasa.gov/gcn/gcn3/3136.gcn3
Fynbo, J. U., et al. 2001, A&A, 369, 373
———. 2005b, GCN Circ. 3176, http://gcn.gsfc.nasa.gov/gcn/gcn3/3176.gcn3

Gehrels, N., et al. 2004, ApJ, 611, 1005
Ghirlanda, G., Ghisellini, G., Firmani, C., Celotti, A., & Bosnjak, Z. 2005, MNRAS, 360, L45
Goad, M., et al. 2005a, GCN Circ. 3032, http://gcn.gsfc.nasa.gov/gcn/gcn3/3032.gcn3
———. 2005b, GCN Circ. 3034, http://gcn.gsfc.nasa.gov/gcn/gcn3/3034.gcn3
Godet, O., et al. 2005, GCN Circ. 3301, http://gcn.gsfc.nasa.gov/gcn/gcn3/3301.gcn3
Golenetskii, S., et al. 2005, GCN Circ. 3179, http://gcn.gsfc.nasa.gov/gcn/gcn3/3179.gcn3
Hullinger, D., et al. 2005, GCN Circ. 3038, http://gcn.gsfc.nasa.gov/gcn/gcn3/3038.gcn3
Kelson, D. D. 2003, PASP, 115, 688
Kelson, D., & Berger, E. 2005a, GCN Circ. 3100, http://gcn.gsfc.nasa.gov/gcn/gcn3/3100.gcn3
———. 2005b, GCN Circ. 3101, http://gcn.gsfc.nasa.gov/gcn/gcn3/3101.gcn3
Kommers, J. M., Lewin, W. H. G., Kouveliotou, C., van Paradijs, J., Pendleton, G. N., Meegan, C. A., & Fishman, G. J. 2000, ApJ, 533, 696
Krimm, H., et al. 2005a, GCN Circ. 3105, http://gcn.gsfc.nasa.gov/gcn/gcn3/3105.gcn3
———. 2005b, GCN Circ. 3119, http://gcn.gsfc.nasa.gov/gcn/gcn3/3119.gcn3
———. 2005c, GCN Circ. 3134, http://gcn.gsfc.nasa.gov/gcn/gcn3/3134.gcn3
———. 2005d, GCN Circ. 3183, http://gcn.gsfc.nasa.gov/gcn/gcn3/3183.gcn3
Lamb, D. Q., et al. 2004, Nucl. Phys. B, 132, 279
Lazzati, D., Covino, S., & Ghisellini, G. 2002, MNRAS, 330, 583
Mangano, V., et al. 2005, GCN Circ. 3253, http://gcn.gsfc.nasa.gov/gcn/gcn3/3253.gcn3
Markwardt, C. B., Boyd, P., Gehrels, N., Hurley, K., Marshall, F. E., & Still, M. 2005, GCN Circ. 3112, http://gcn.gsfc.nasa.gov/gcn/gcn3/3112.gcn3
McNaught, R., et al. 2005, GCN Circ. 3163, http://gcn.gsfc.nasa.gov/gcn/gcn3/3163.gcn3
Misra, K., et al. 2005, GCN Circ. 3226, http://gcn.gsfc.nasa.gov/gcn/gcn3/3226.gcn3
Mitani, T., et al. 2005, GCN Circ. 3055, http://gcn.gsfc.nasa.gov/gcn/gcn3/3055.gcn3
Monfardini, A., et al. 2005, GCN Circ. 3001, http://gcn.gsfc.nasa.gov/gcn/gcn3/3001.gcn3
Mulchaey, J., & Berger, E. 2005, GCN Circ. 3114, http://gcn.gsfc.nasa.gov/gcn/gcn3/3114.gcn3
Nakagawa, Y., et al. 2005, GCN Circ. 3053, http://gcn.gsfc.nasa.gov/gcn/gcn3/3053.gcn3
Nysewander, M., et al. 2005, GCN Circ. 3067, http://gcn.gsfc.nasa.gov/gcn/gcn3/3067.gcn3
Piro, L. 2001, in AIP Conf. Proc. 599, X-Ray Astronomy: Stellar Endpoints, AGN, and the Diffuse X-Ray Background, ed. N. E. White, G. Malaguti, & G. G. C. Palumbo (Melville: AIP), 295
Price, P. A., et al. 2005a, GCN Circ. 3164, http://gcn.gsfc.nasa.gov/gcn/gcn3/3164.gcn3
———. 2005b, GCN Circ. 3313, http://gcn.gsfc.nasa.gov/gcn/gcn3/3313.gcn3
Sakamoto, T., et al. 2005a, ApJ, 629, 311
———. 2005b, GCN Circ. 3189, http://gcn.gsfc.nasa.gov/gcn/gcn3/3189.gcn3
———. 2005c, GCN Circ. 3273, http://gcn.gsfc.nasa.gov/gcn/gcn3/3273.gcn3
———. 2005d, GCN Circ. 3305, http://gcn.gsfc.nasa.gov/gcn/gcn3/3305.gcn3
Sato, G., et al. 2005a, GCN Circ. 2987, http://gcn.gsfc.nasa.gov/gcn/gcn3/2987.gcn3
———. 2005b, GCN Circ. 3284, http://gcn.gsfc.nasa.gov/gcn/gcn3/3284.gcn3

Soderberg, A. M., & Frail, D. A. 2005, GCN Circ. 3092, http://gcn.gsfc.na-sa.gov/gcn/gcn3/3092.gcn3

Soderberg, A. M., et al. 2005a, GCN Circ. 3035, http://gcn.gsfc.nasa.gov/gcn/gcn3/3035.gcn3

———. 2005b, GCN Circ. 3066, http://gcn.gsfc.nasa.gov/gcn/gcn3/3066.gcn3

———. 2005c, GCN Circ. 3102, http://gcn.gsfc.nasa.gov/gcn/gcn3/3102.gcn3

———. 2005d, GCN Circ. 3127, http://gcn.gsfc.nasa.gov/gcn/gcn3/3127.gcn3

———. 2005e, GCN Circ. 3132, http://gcn.gsfc.nasa.gov/gcn/gcn3/3132.gcn3

———. 2005f, GCN Circ. 3187, http://gcn.gsfc.nasa.gov/gcn/gcn3/3187.gcn3

———. 2005g, GCN Circ. 3223, http://gcn.gsfc.nasa.gov/gcn/gcn3/3223.gcn3

———. 2005h, GCN Circ. 3234, http://gcn.gsfc.nasa.gov/gcn/gcn3/3234.gcn3

———. 2005i, GCN Circ. 3277, http://gcn.gsfc.nasa.gov/gcn/gcn3/3277.gcn3

———. 2005j, GCN Circ. 3308, http://gcn.gsfc.nasa.gov/gcn/gcn3/3308.gcn3

———. 2005k, GCN Circ. 3318, http://gcn.gsfc.nasa.gov/gcn/gcn3/3318.gcn3

Tanvir, N., et al. 2005a, GCN Circ. 3028, http://gcn.gsfc.nasa.gov/gcn/gcn3/3028.gcn3

Tanvir, N., et al. 2005b, GCN Circ. 3031, http://gcn.gsfc.nasa.gov/gcn/gcn3/3031.gcn3

Tristram, P., Jelinek, M., de Ugarte Postigo, A., Gorosabel, J., Castro-Tirado, A. J., Castro Ceron, J. M., & Yock, P. 2005, GCN Circ. 3151, http://gcn.gsfc .nasa.gov/gcn/gcn3/3151.gcn3

Tueller, J., et al. 2004, GCN Circ. 2898, http://gcn.gsfc.nasa.gov/gcn/gcn3/2898.gcn3

———. 2005, GCN Circ. 3251, http://gcn.gsfc.nasa.gov/gcn/gcn3/3251.gcn3

Vanderspek, R., Villaseñor, J., Doty, J., Jernigan, J. G., Levine, A., Monnelly, G., & Ricker, G. R. 1999, A&AS, 138, 565

Vanderspek, R., et al. 2004, ApJ, 617, 1251

Wells, A. A., et al. 2005, GCN Circ. 3191, http://gcn.gsfc.nasa.gov/gcn/gcn3/3191.gcn3

Wieringa, M. H., et al. 2005, GCN Circ. 3098, http://gcn.gsfc.nasa.gov/gcn/gcn3/3098.gcn3